Steady fall of isothermal, resistive-viscous, compressible fluid across magnetic field

B. C. Low[1] and A. K. Egan[2]

[1)] *High Altitude Observatory, National Center for Atmospheric Research, Boulder, Colorado*

[2)] *Barnard College, New York, New York & Department of Physics, Colorado University, Boulder, Colorado*

(Submitted to J. Physics of Plasmas, March 7 2014)

This is a basic MHD study of the steady fall of an infinite, vertical slab of isothermal, resistive-viscous, compressible fluid across a dipped magnetic field in uniform gravity. This double-diffusion steady flow in unbounded space poses a nonlinear but numerically tractable, one-dimensional (1D) free-boundary problem, assuming constant coefficients of resistivity and viscosity. The steady flow is determined by a dimensionless number μ_1 proportional to the triple product of the two diffusion coefficients and the square of the linear total mass. For a sufficiently large μ_1, the Lorentz, viscous, fluid-pressure, and gravitational forces pack and collimate the fluid into a steady flow of a finite width defined by the two zero-pressure free-boundaries of the slab with vacuum. The viscous force is essential in this collimation effect. The study conjectures that in the regime $\mu_1 \to 0$, the 1D steady state exists only for $\mu_1 \in \Omega$, a spectrum of an infinite number of discrete values, including $\mu_1 = 0$ that corresponds to two steady states, the classical zero-resistivity static slab of Kippenhahn & Schlüter[1] and its recent generalization[2] to admit an inviscid resistive flow. The pair of zero-pressure boundaries of each of the $\mu_1 \to 0$ steady-state slabs are located at infinity. Computational evidence suggests that the Ω steady-states are densely distributed around $\mu_1 = 0$, as an accumulation point, but are sparsely separated by open intervals of μ_1-values for which the slab must be either time-dependent or spatially multi-dimensional. The widths of these intervals are vanishingly small as $\mu_1 \to 0$. This topological structure of physical states is similar to that described by Landau & Liftshitz[3] to explain the onset of hydrodynamic turbulence. The implications of this MHD study are discussed, with an interest in the prominences in the solar atmosphere and the interstellar clouds in the Galaxy.

I. INTRODUCTION

This is a theoretical study of the descent of a vertical slab of electrically-resistive, viscous, compressible, isothermal fluid across a horizontally oriented magnetic field dipped by the weight of the fluid. We treat a one-dimensional (1D) free-boundary problem posed by an infinite slab in unbounded space to investigate a novel family of steady resistive-viscous flows. A global nonlinear interplay among the Lorentz, fluid-pressure, viscous and gravitational forces determines whether a 1D steady state may exist and, when a steady state does exist, whether the slab's pair of zero-pressure boundaries meet with vacuum at finite distances or at infinity. Despite its geometric simplicity, our slab model illustrates quite complex physical properties in the manner of several similarly instructive MHD models in the journal literature[1,4–7].

The magnetic suspension of a slab of fluid in gravity is central to understanding quiescent prominences in the Sun's outer atmosphere, the corona[8–16]. Prominences described as quiescent are a common variety found in the corona on any day. These are large-scale, long-lived partially-ionized condensations two orders of magnitude cooler and denser than the fully-ionized, million-degree hot corona. Such a prominence is invariably an elongated structure aligned with and running horizontally right above a polarity-reversal line on the solar surface, a line separating two large regions of opposite vertical components of the surface field. Recent observations from spacecrafts have for the first time the necessary spectral, spatial and temporal resolutions to directly image the turbulent interior of a prominence, revealing curtains of closely-spaced, dense, cool (10^4 K), narrow prominence threads descending at less than the gravitational free-fall speed; see Figure 1[12,13]. These threads are interspersed amidst equally-narrow, upward vertical streams of hot ($10^5 - 10^6$ K) tenuous plasma, suggesting a novel magneto-thermal convective process[17,18]. Spectral-polarimetric observations have long indicated that the magnetic fields are horizontal in the cool interior of prominences[19–21]. The relative absence of a downward acceleration of the descending threads can be explained in terms of the canceling of the the gravitational force by a Lorentz force acting upward perpendicular to the inferred field. This has led to the intriguing hypothesis that, in spite of high electrical conductivity in the prominence, the cool plasma threads are falling resistively across their horizontally-oriented supporting fields[2,17,22–26].

Extremely-thin current sheets form naturally under conditions of extremely-high elec-

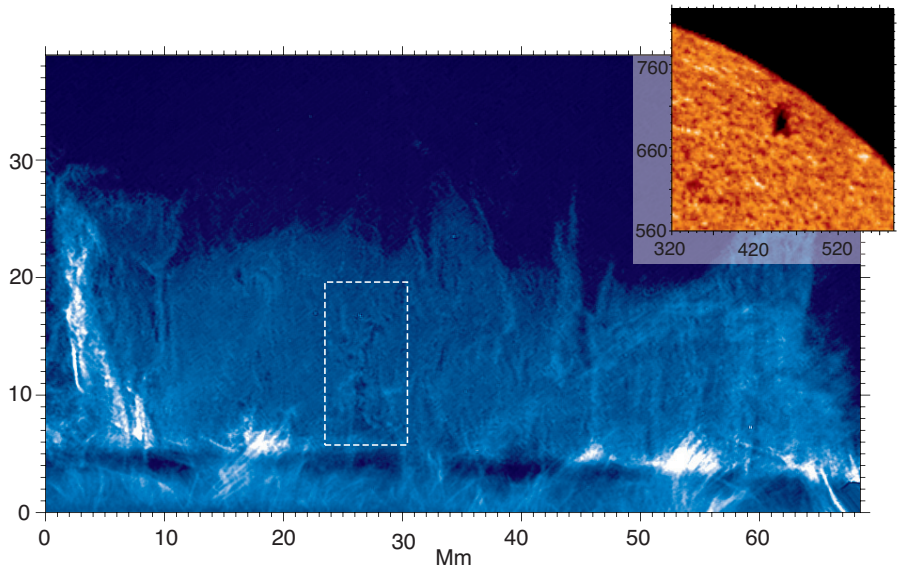

FIG. 1. Quiescent prominence in main figure observed on 2006 November 30 in Ca ii H-line 396.8 nm emission in the northern solar corona above the projected edge of the Sun[13]. Against the dark sky, the prominence displays ubiquitous vertical threads of cool dense plasma in emission descending amidst upward flows observed as equally-narrow dark lanes; see the two-component structure in the region identified by the white dashed box. The insert figure is an H_α image showing this prominence as a dark absorption structure against the bright solar disk. The main and insert figures are images from the Solar Optical Telescope onboard the *Hinode* spacecraft and the Mauna Loa Solar Observatory, respectively.

trical conductivity in the course of a three-dimensional magnetic field evolving with an invariant complex topology, as pointed out by Parker[27–31]. In addition to this general effect, extremely thin current sheets also develop dynamically to accommodate energy transport involving highly-anisotropic thermal conduction in the coronal-prominence environment[26]. From these theoretical considerations, resistive flows may be a common occurrence, resulting from the spontaneous formation and dissipation of the current sheets. This dynamical mode of resistive dissipation is thus actually a direct consequence of high electrical conductivity[28]. If the hypothesized resistive origin of prominence down-flows is accepted, it is intriguing to note from observations that the descending prominence threads may drain away, in about a day, an order of magnitude more mass than the quasi-steady total mass residing in a prominence at any one time[25]. The Parker[32–36] hydromagnetic instability in a gravitationally

stratified atmosphere was originally proposed to explain the formation of long-lived interstellar clouds suspended in the large-scale magnetic field of our Galaxy. The prominences are of the same hydromagnetic origin[18] and the recent solar observations, described above, suggest that resistive down-flows may also be an integral component of interstellar-cloud formation.

Our study is motivated by the possible resistive origin of the descending prominence threads. In Section 2 we concentrate on the steady resistive-viscous flow of a fluid across its embedded magnetic field as a basic MHD process. The results obtained are summarized and discussed in Section 3, both for their basic physics and in relation to the phenomena of prominences and interstellar clouds. The cgs units are used in this paper.

II. THE RESISTIVE VISCOUS SLAB

Consider the one-fluid MHD equations describing a resistive viscous fluid:

$$\rho\left[\frac{\partial \mathbf{v}}{\partial t}+(\mathbf{v}\cdot\nabla)\,\mathbf{v}\right]=\frac{1}{4\pi}(\nabla\times\mathbf{B})\times\mathbf{B}-\nabla p-\rho g\hat{z} \\ -\nabla\times(\mu\nabla\times\mathbf{v})+\nabla\left[(\mu-\frac{2}{3}\nu)\nabla\cdot\mathbf{v}\right], \tag{1}$$

$$\frac{\partial \rho}{\partial t}+\nabla\cdot(\rho\mathbf{v})=0, \tag{2}$$

$$\frac{\partial \mathbf{B}}{\partial t}=\nabla\times(\mathbf{v}\times\mathbf{B}-\eta\nabla\times\mathbf{B}), \tag{3}$$

where p, ρ, $\mathbf{v}$, and $\mathbf{B}$ are the pressure, density, velocity and magnetic field, respectively. The dissipative coefficients, μ and ν for viscosity and η for resistivity, are taken to be constants. Gravitational acceleration g is uniform and directed opposite to the vertical unit vector $\hat{z}$ in Cartesian coordinate system (x, y, z). An equation of energy transport is needed to close this set of MHD equations. To keep the physical problem simple, we impose the isothermal condition, defining the uniform temperature $T = T_0$ by the ideal gas law

$$p=\frac{\rho k_B T_0}{m_0}, \tag{4}$$

where k_B and m_0 are the Boltzmann constant and molecular mass, respectively.

We are interested in a steady vertical slab of fluid of infinite extent in the directions of igonorable coordinates (z, x), with all physical quantities depending on only coordinate y.

This slab falls vertically with velocity $\mathbf{v} = v(y)\hat{z}$ and embeds a magnetic field of the form

$$\mathbf{B} = B_0 \left[0, 1, H(y)\right], \tag{5}$$

$$\nabla \times \mathbf{B} = B_0 \frac{dH}{dy}\hat{x}, \tag{6}$$

B_0 being a free constant. The field lines are identical curves in the $y - z$ plane described by

$$\frac{dz}{dy} = H(y). \tag{7}$$

In 3D physical space, the density $\rho(y)$ is 1D but the slab is threaded by these geometrically 2D field lines.

The three variables (ρ, v, H) describe the slab, with pressure p proportional to ρ under the isothermal condition. We have $\mathbf{v} \cdot \nabla \equiv 0$ and $\nabla \cdot \mathbf{v} = 0$, so momentum equation (1) reduces to the respective y and z components:

$$p + \frac{B_0^2}{8\pi} H^2 = \frac{B_0^2}{8\pi} H_0^2, \tag{8}$$

$$\frac{B_0^2}{4\pi}\frac{dH}{dy} - \rho g + \frac{d}{dy}\left(\mu \frac{dv}{dy}\right) = 0, \tag{9}$$

where we have integrated for pressure p, H_0 arising as an integration constant. Equation (8) shows that the slab is confined horizontally by the magnetic pressure contributed by B_z. The magnetic-tension and viscous forces are everywhere vertical and Equation (9) describes the balance of the weight of the fluid by these two forces. Mass-conservation equation (2) is trivially satisfied. Induction equation (3) integrates to give

$$v = -\eta \frac{dH}{dy} + v_0, \tag{10}$$

where v_0 is an integration constant. MHD is a Galilean-invariant Newtonian description. Any two inertial frames moving at a constant relative velocity observe the same MHD phenomena. We may set $v_0 = 0$ with no loss of generality to obtain

$$v = -\eta \frac{dH}{dy} \tag{11}$$

in a suitably defined inertial frame. Equations (8), (9), and (11) are a complete set to determine (ρ, v, H), again noting that p is proportional to ρ.

Substituting for p and v in favor of H, Equation (9) gives

$$\frac{B_0^2}{4\pi}\frac{dH}{dy} - \frac{B_0^2}{8\pi}\frac{m_0 g}{k_B T_0}\left(H_0^2 - H^2\right) - \frac{d}{dy}\left[\mu \frac{d}{dy}\left(\eta \frac{dH}{dy}\right)\right] = 0, \tag{12}$$

a third-order ordinary differential equation (ODE). The slab could be of an infinite width, meaning that $\rho(y)$ is defined everywhere on the y axis, with $\rho \to 0$ as $y \to \pm\infty$. We must also allow for a compressible fluid to be packed by the forces into a slab of a finite width, that is, the $\rho = 0$ boundaries are located at finite distances. The coordinate y does not appear explicitly in ODE (12), so its solution $H(y)$ is translationally invariant. One of the three integration constants defining a particular solution $H(y)$ can be fixed by locating the origin $y = 0$ at any chosen point relative to the slab. With no loss of generality, then, we may locate the boundaries $\rho = 0$ at $y = \pm y_1$. Then the solution $H(y)$ contains only two free constants of integration.

The steady slab with a finite width may be regarded to have gravitationally collapsed[32,35] from an initial state in which $\rho \neq 0$ everywhere. The evacuation of mass creates the external vacuum regions $y_1 < |y| < \infty$, leaving behind the oppositely-inclined (potential) uniform fields

$$\mathbf{B} = B_0 \left[0, 1, \pm H_0\right], \tag{13}$$

in $y > y_1$ and $y < -y_1$, respectively, taking B_0 and H_0 positive. These external fields are deduced by noting that B_y is continuous at $y = \pm y_1$ by the solenoidal condition and that $p = 0, B_z = \pm B_0 H_0$ at $y = \pm y_1$, respectively. The slab cannot exert any frictional force on vacuum, so the net frictional force is zero, expressed by the stress-free boundary conditions:

$$y = \pm y_1, \quad \mu \frac{dv}{dy} = 0. \tag{14}$$

In general, $v \neq 0$ at $y = \pm y_1$ describing the downward steady fall of these boundaries adjacent to vacuum. These considerations impose the boundary conditions

$$y = \pm y_1, \quad H = \pm H_0, \qquad \frac{d^2 H}{dy^2} = 0, \tag{15}$$

where we have used Equation (11). If y_1 is arbitrarily prescribed, we would have an over specification of imposing four boundary conditions on the solution $H(y)$ that has only two integration constants. This difficulty is resolved by realizing we have a free boundary problem (FBP) that treats y_1 as an unknown constant to be solved together with $H(y)$, the subject of investigation in this Section.

A. The free-boundary problem

Let us formulate the FBP in dimensionless form for a slab $|y| < y_1$, symmetric about its central plane $y = 0$, i.e., $\rho(y)$ is an even function. Inspection of the governing equations (8), (9) and (11) shows that $v(y)$ and $H(y)$ are even and odd functions, respectively. We also have $H(0) = 0$. Use the normalizations:

$$P = p/p_0, \quad D = \rho/\rho_0, , \quad [X, Y, Z] = \Lambda_0^{-1}[x, y, z], \tag{16}$$

where $\Lambda_0 = \frac{k_B T_0}{m_0 g}$ is the isothermal hydrostatic scale-height. Define $p_0 = p(0)$, so that $P(0) = 1$, and introduce the constant plasma parameter $\beta = 8\pi p_0/B_0^2$. An important note is that the ratio of fluid to magnetic pressure varies in space and β so defined is the particular value of that ratio at slab center $y = 0$ *in the steady state*. For a given p_0, the ideal gas law (4) gives $p_0 = \rho_0 k T_0/m_0$, defining the constant ρ_0 in terms of p_0 and T_0. We thus have the dimensionless ideal gas law, $P = D$. With $p(0) = p_0, H(0) = 0$ and $p(\pm y_1) = 0, H(\pm y_1) = \pm H_0$, Equation (8) gives

$$H(\pm Y_1) = \pm H_0 = \pm \beta^{1/2}, \tag{17}$$

where $Y_1 = \Lambda_0^{-1} y_1$.

These considerations suggest the following useful variables:

$$h(Y) = \beta^{-1/2} H(y), \tag{18}$$

$$\begin{aligned} u(Y) &= \Lambda_0 \beta^{-1} \frac{dH}{dy} \\ &= \beta^{-\frac{1}{2}} \frac{dh}{dY}, \end{aligned} \tag{19}$$

being the dimensionless forms of the vertical field-component B_z and the current-density in the x direction; see Equations (5) and (6). The governing equations (8) and (11) transform into the algebraic equations:

$$D = P = 1 - h^2, \tag{20}$$

$$v = -\frac{\eta\sqrt{\beta}}{\Lambda_0} \frac{dh}{dY} = -v_\eta \beta u. \tag{21}$$

If $\eta = 0$, the resistive velocity $v = 0$ whereas the current-density $u \neq 0$ generally, so it is useful to keep the physical meanings of v and u distinct. There are three characteristic

speeds, resistive diffusion-speed $v_\eta = \eta/\Lambda_0$ introduced in Equation (21), viscous diffusion-speed $v_\mu = \mu/(\Lambda_0\rho_0)$, and Alfven speed $v_A = B_0/\sqrt{4\pi\rho_0}$. Substituting D and v in favor of h in ODE (9), we obtain the dimensionless form of ODE (12):

$$2\frac{dh}{dY} - \sqrt{\beta}(1-h^2) - 2\mu_0\frac{d^3h}{dY^3} = 0, \tag{22}$$

where the three characteristic speeds are combined into the dimensional number

$$\mu_0 = \frac{v_\eta v_\mu}{v_A^2} = 4\pi\frac{\eta\mu}{\Lambda_0^2 B_0^2}. \tag{23}$$

Boundary conditions (15) transform into

$$\text{at } Y = \pm Y_1, \quad h = \pm 1, \qquad \frac{d^2h}{dY^2} = 0. \tag{24}$$

In the FBP posed by Equations (22) and (24), Y_1 is an unknown, as pointed out earlier.

Consider the linear total mass in the steady state:

$$\begin{aligned} M_T &= \int_{-y_1}^{y_1} \rho \, dy \\ &= \frac{B_0^2}{8\pi g}\beta \int_{-Y_1}^{Y_1} \left[1 - h(Y)^2\right] \, dY, \end{aligned} \tag{25}$$

using Equation (20) to express ρ in terms of h. ODE (9) describing the support of the weight of the fluid by the tension and viscous forces admits an explicit relationship among the four constants (M_T, β, g, B_0). Integrate this ODE across the width of the slab, subject to boundary conditions (14) and (15), to obtain:

$$\begin{aligned} M_T g &= \frac{B_0^2}{2\pi} H_0 \\ &= \frac{B_0^2}{2\pi}\beta^{1/2}, \end{aligned} \tag{26}$$

recalling Equation (17) that $H_0 = \beta^{1/2}$. We have shown that β, the ratio of fluid to magnetic pressure at slab center $Y = 0$, is fixed by (M_T, g, B_0):

$$\beta = \left(\frac{2\pi M_T g}{B_0^2}\right)^2. \tag{27}$$

Each physical realization of the 1D system is specified by giving the values of $(M_T, T_0, g, B_0, \eta, \mu)$ as the invariant properties of the system. The FBP may then be articulated to be seeking the steady state for a slab of (linear) total mass M_T that has deformed a given initial horizontal field $\mathbf{B}_{initial} = B_0\hat{y}$ into the dipped field $\mathbf{B} = B_0\left[\hat{y} + H(y)\hat{z}\right]$, such that a vertical

steady flow is maintained via a balance among the four forces. In an evolution to a steady state, M_T is conserved as $\rho(y,t)$ evolves dynamically with time-dependent fluid-boundaries where $\rho(y,t)=0$. When a steady state $[\rho(y), v(y), H(y)]$ has been attained, this state is described by ODE (22) and boundary conditions (24), with (μ_0, β) fixed by Equations (23) and (27) in terms of the invariant properties of the system. In particular, the locations of the steady-state fluid-boundaries $Y = \pm Y_1$ are then related to the field solution h by the integral equation:

$$\sqrt{\beta}\int_{-Y_1}^{Y_1} \left[1-h(Y)^2\right]\, dY = 4, \tag{28}$$

obtained from Equations (25) and (27). The coupled equations, ODE (22) and integral equation (28), subject to boundary conditions (24) pose a FBP for $h(y)$ and Y_1 as the unknowns.

B. Equivalent boundary-value problem in h-space

In the symmetric steady slab, $h(Y) = \beta^{-1/2}H(y)$ is a monotonically increasing odd function in the domain $-Y_1 < Y < Y_1$ with $h(\pm Y_1) = \pm 1$. Therefore, $h(Y)$ maps the domain $-Y_1 < Y < Y_1$ onto $-1 < h < 1$. The FBP for $h(Y)$ can be solved as an equivalent boundary-value problem (BVP) for current-density u, defined by Equations (19), as a function of h in the domain $-1 < h < 1$. The formula $\frac{du}{dY} = \sqrt{\beta}u\frac{du}{dh}$ transforms ODE (22) into

$$\mu_1 u\frac{d^2u^2}{dh^2} - 2u + 1 - h^2 = 0, \tag{29}$$

with a single constant parameter

$$\mu_1 = \beta\mu_0 = 4\pi\frac{\beta\eta\mu}{\Lambda_0^2 B_0^2}, \tag{30}$$

in terms of the invariant properties of the physical system. Substituting for $\frac{d^2h}{dY^2} = \beta u\frac{du}{dh}$ in boundary conditions (24) we obtain

$$h = -1, 1, \quad \frac{du^2}{dh} = 0, \tag{31}$$

which together with the ODE (29) posed a BVP for $u(h)$.

This BVP has an awkward feature, posing boundary conditions on u^2, whereas u is the independent variable in ODE (29), requiring care when $u \to 0$; see Sub-section (II E) and

Appendix A. In the numerical computations carried out, we solve the equivalent BVP for $q = u^2$:

$$\mu_1 q^{1/2} \frac{d^2 q}{dh^2} - 2q^{1/2} + 1 - h^2 = 0, \tag{32}$$

$$h = -1, 1, \quad \frac{dq}{dh} = 0. \tag{33}$$

For discussing physics, it is useful to stay with current-density u as the dependent variable of ODE (29).

Unless stated otherwise, let us assume $u \neq 0$ so that $\frac{du^2}{dh} = 0$ is equivalent to $\frac{du}{dh} = 0$ and, for the symmetric slab, we solve ODE (29) subject to the boundary conditions for the half-slab,

$$h = 0, 1, \quad \frac{du}{dh} = 0. \tag{34}$$

Each solution $u(h)$ of this BVP, solved without knowledge of Y_1, gives $h(Y)$ by Equation (19) in the implicit form,

$$Y = \int_0^h \frac{dh'}{\sqrt{\beta} u(h')}, \tag{35}$$

in terms of which all physical quantities are expressed as functions of Y. The locations of the slab boundaries $Y = \pm Y_1$ are also determined,

$$Y_1 = \int_0^1 \frac{dh'}{\sqrt{\beta} u(h')}, \tag{36}$$

in this final separate step. Thus we have decoupled the two unknown Y_1 and $h(Y)$ in the FBP.

For each BVP solution with $u \neq 0$ at $h = \pm 1$, integral (36) gives a finite Y_1, i.e., the slab has a finite thickness $2Y_1$. Later we will encounter cases of $u \to 0$ at $h = \pm 1$. For example, u may go to zero as $(1 - |h|)^m$ as $h \to \pm 1$, m a positive constant. Then the slab thickness is finite only if $0 < m < 1$. In particular, integral (36) is logarithmically divergent if $m = 1$, a case of an infinite slab-thickness with the free boundaries $P = 0$ located at infinity.

Finally, we present an exact integral of ODE (29), the mass function $m[h(y)]$ defined in physical space by

$$M_T m[h(y')] = \int_{-y'}^{y'} \rho(y)\, dy, \tag{37}$$

where M_T is the total linear mass given by Equation (25). That is, $m[h(y')]$ is the linear total mass enclosed between a pair of symmetric planes $y = \pm y'$ in the slab as a fraction of

M_T; by definition $y' \leq y_1$ and $m[h(y_1)] = m(1) = M_T$. In h-space, Equation (37) gives

$$\frac{dm(h)}{dh} = \frac{1}{2}\frac{D(h)}{u(h)} = \frac{1}{2}\frac{1-h^2}{u(h)}. \tag{38}$$

Divide by u across ODE (29) and then integrate from $h = 0$ to an arbitrary point h in the half-domain $0 < h < 1$ to obtain

$$m(h) = h - \frac{1}{2}\mu_1 \frac{du^2}{dh}, \tag{39}$$

where we have imposed $\frac{du}{dh} = 0$ at $h = 0$ under boundary conditions (34). Numerical methods are the only practical means of solving the nonlinear ODE (29). Exact formula (39) for $m(h)$ is useful both as a check on the accuracy of numerical solutions and as a guide in the physical interpretation of these solutions.

C. Numerical solutions

We have carried out numerical solution of the BVP (29) and (34) using a fourth-order Runge-Kutta solver in a shooting method, proceeding with simultaneous solution of the auxiliary ODEs

$$\frac{dY}{dh} = \frac{1}{\sqrt{\beta}u(h)}, \tag{40}$$

$$\frac{dZ}{dh} = \frac{h}{\sqrt{\beta}u(h)}, \tag{41}$$

for $h(Y)$ and the field-line equation $Z = Z[h(Y)]$. Appendix A gives the essential details of this numerical computation. For a given value of μ_1, the Runge-Kutta integrations of ODE (29) towards $h = 1$ from $h = 0$ starts with prescribed initial conditions $u(0) = u_0$, $\frac{du}{dh} = 0$, varying the trial constant u_0 to "shoot" iteratively for a value that allows a solution to arrive at $h = 1$ with zero gradient required by boundary conditions (34). Figures 2 and 3 display the four cases with $\beta = 1.0$ and $\mu_1 = 2.0, 0.4, 0.1, 0.066$ in decreasing magnitudes. Shown for each case are a set of trial numerical solutions $u(h)$ in the half domain $0 < h < 1$ that sample the function-space of solutions symmetric about $h = 0$ in the whole domain $-1 < h < 1$. These sets provide a first look at the mathematical nature of the nonlinear ODE (29) with its singularity points where $u = 0$. Singularity points are defined to be points on the $h - u$ plane where the coefficient of the highest derivative in the ODE vanishes.

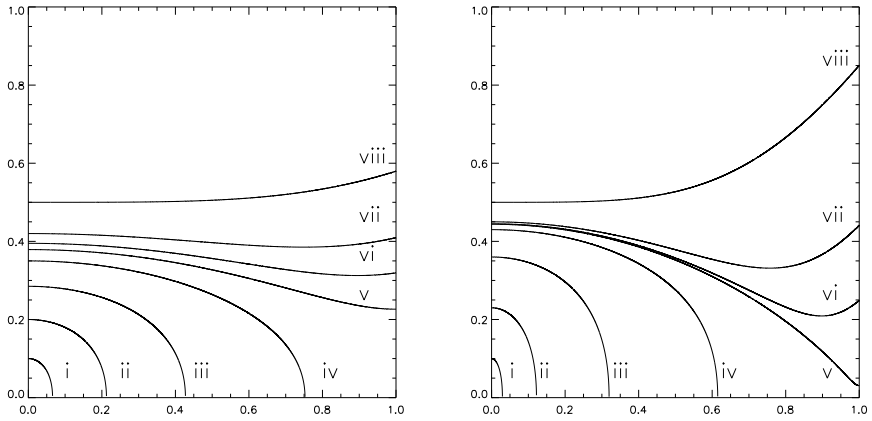

FIG. 2. Runge-Kutta solutions $u(h)$ with $0 < h < 1$ on the abscissa, generated by a shooting method for $\mu_1 = 2.0$ (left) with the starting values of $u_0 = u(0)$ at $h = 0$: (i) 0.1, (ii) 0.2, (iii) 0.285, (iv) 0.35, (v) 0.379, (vi) 0.395, (vii) 0.42, (viii) 0.5, as labelled; and, for $\mu = 0.4$ (right) with the starting values of $u_0 = u(0)$ at $h = 0$: (i) 0.1, (ii) 0.23, (iii) 0.36, (iv) 0.43, (v) 0.44389, (vi) 0.445, (vii) 0.45, (viii) 0.5, as labelled. In each case, the solution labelled (v), defined for the entire domain $0 < h < 1$ with zero gradient at the two end-points, is a solution of the BVP posed by ODE (29) and homogeneous boundary conditions (34).

The two sets of trial solutions for $\mu_1 = 2.0, 0.4$ in Fig. 2 have the following property. In each set, for a sufficiently small initializing trial value of $u_0 = u(0)$, the trial solution $u(h)$ monotonically decreases from u_0 as its maximum at $h = 0$ to zero at a singularity point $h = h_1 < 1$. Specifically, $u \propto (h_1 - h)^{1/2}$ as $h \to h_1$, shown in Appendix A. The solution is not defined for $h > h_1$. For a sufficiently large u_0, $u(h) \neq 0$ in the entire domain $0 < h < 1$. The shapes of these everywhere nonzero solutions belong to one of three classes: (A) $u(h)$ is a monotonically increasing function with u_0 as a local minimum at $h = 0$, (B) $u(h)$ decreases monotonically from u_0 as a local maximum at $h = 0$ to a local (zero-gradient) minimum located well within domain $0 < h < 1$, and (C) $u(h)$ decreases monotonically from u_0 as a local maximum at $h = 0$ to a minimum value located right at the end-point $h = 1$ where its gradient is negative. A critical value of u_0 gives a solution $u(h)$ separating classes (B) and (C), labelled as curve (V) in both sub-figures of Fig. 2. This critical solution decreases monotonically from u_0 as a local maximum at $h = 0$ to a zero-gradient minimum value located right at the end-point $h = 1$ and it is the solution to the BVP posed by Equations

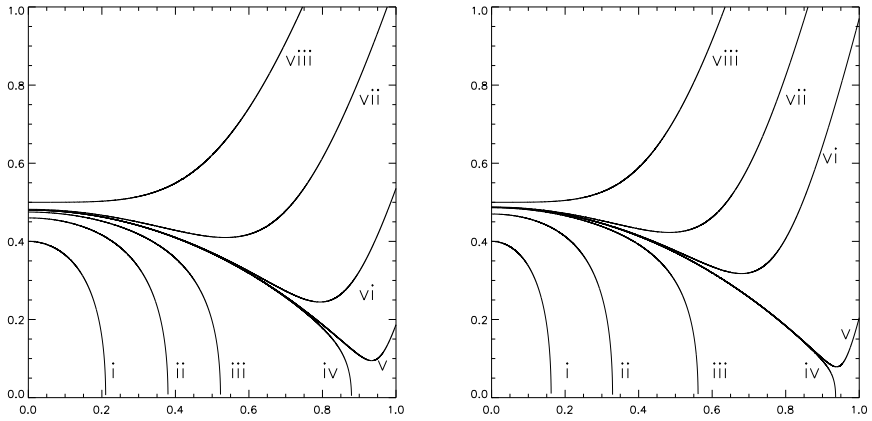

FIG. 3. Runge-Kutta solutions $u(h)$ with $0 < h < 1$ on the abscissa, generated by a shooting method for $\mu_1 = 0.1$ (left) with the starting values of $u_0 = u(0)$ at $h = 0$: (i) 0.4, (ii) 0.46, (iii) 0.475, (iv) 0.479920, (v) 0.479928, (vi) 0.480, (vii) 0.486, (viii) 0.5, as labelled; and, for $\mu = 0.066$ (right) with the starting values of $u_0 = u(0)$ at $h = 0$: (i) 0.4, (ii) 0.470, (iii) 0.486, (iv) 0.487023180, (v) 0.487023193, (vi) 0.4871, (vii) 0.4880, (viii) 0.5, as labelled. In each case, there is no solution defined for the entire domain $0 < h < 1$ with zero gradient at the two end-points, i.e., the BVP posed by ODE (29) and homogeneous boundary conditions (34) has no solution for these two values of μ_1.

(29) and (34) we seek in the two cases of $\mu_1 = 2.0, 0.4$ shown.

The two sets of trial solutions for the smaller values $\mu_1 = 0.1, 0.066$ in Fig. 3 show a significant difference from the two sets in Fig. 2. In each set in Fig. 3, a sufficiently small $u_0 = u(0)$ generates a trial function $u(h)$ vanishing as $(h_1 - h)^{1/2}$ at some point $h = h_1 < 1$, whereas the larger values of u_0 produce everywhere nonzero $u(h)$ only of shapes belonging to classes (A) and (B). No nonzero $u(h)$ of class (C) could be found within the numerical capability of the Runge-Kutta computational code in use. The implication follows that the BVP posed by Equations (29) and (34) has no solution for $\mu_1 = 0.1, 0.066$ unless, possibly, the BVP-solution exists with both $u(h)$ and its gradient vanishing at end point $h = 1$. Suppose we assume that the solution $u(h)$ of the BVP exists everywhere in the parametric range $0.066 < \mu_1 < 2.0$. An inspection of the class-(B) trial solutions of the four cases $\mu_1 = 2.0, 0.4, 0.1, 0.066$ in Figs. 2 and 3 supports the conclusion that $u \to 0$ as $h \to 1$ is a necessary, but not sufficient, condition for a BVP-solution to exist in the range $0 < \mu_1 < \mu_c$ where μ_c is a computable critical point within the bounds $0.1 < \mu_c < 0.4$.

All the BVP-solutions in the regime $\mu_1 > \mu_c$ have $u(1) \neq 0$, each describing a slab with a finite width $2Y_1$ given by integral (36). Recall from Equations (23) **and (26)** that $\mu_1 = \beta\mu_0 \propto \eta\mu M_T^2$, the triple product of the coefficients of resistivity and viscosity and M_T^2. Therefore $\mu_1 > \mu_c$ does not necessarily imply that the two diffusion coefficients are large. Even for a weakly resistive and viscous fluid, the combined effect of magnetic-field and velocity diffusion is significant if the linear mass of the fluid is sufficiently large. In contrast, a BVP-solution in the range $\mu_1 < \mu_c$, if it exists, must vanish at end point $h = 1$ so that the integrand of the integral (36) diverges at $h = 1$. It is then to be determined from the nature of that divergence whether the slab-width is finite or infinite.

The range $\mu_1 < \mu_c$ includes the special point $\mu_1 = 0$ obtaining in two distinct cases, one being $\eta = 0$ for which the resistive velocity vanishes and we have the well-known static Kippenhahn-Schluter[1] slab, hereafter called the KS slab. The other case of $\mu_1 = 0$ obtains if $\eta \neq 0$ but $\mu = 0$, for which the resistive velocity is present but is inviscid. This case admits a steady-state as a generalization[2] of the KS slab to allow for a resistive-inviscid velocity. The two $\mu_1 = 0$ special steady states provide a useful comparison with the illustrative explicit resistive-viscous slab in the range $\mu_1 > \mu_c$ we present next. The existence of the $\mu_c > \mu_1 \neq 0$ steady states and the properties of the singularity point $u \to 0$ at $h = 1$ are analyzed in Sub-section (II E).

D. The $\mu_1 > \mu_c$ steady resistive-viscous slabs

We first construct the static KS slab to serve as an interesting $\mu_1 = 0$ reference state and then present a representative, explicit FBP solution for the $\mu_1 > \mu_c$ steady resistive-viscous slab.

1. The KS slab

With $\eta = 0$, the slab is static. ODE (29) becomes an algebraic equation,

$$2u = 1 - h^2, \tag{42}$$

and integral (35) gives

$$h = h_{KS} = \tanh\frac{\sqrt{\beta}}{2}Y. \tag{43}$$

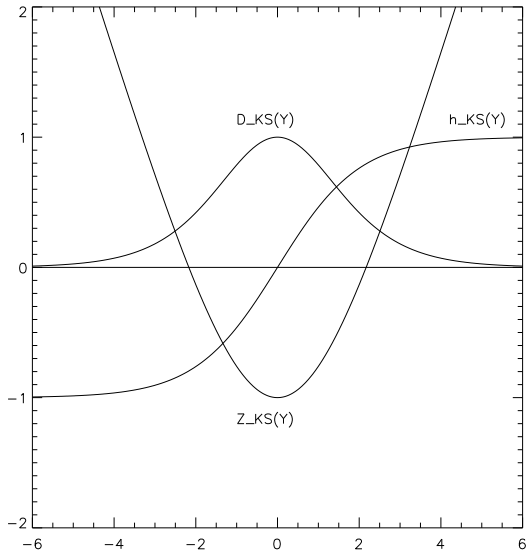

FIG. 4. Static isothermal Kippenhahn-Schlüter perfectly-conducting slab, displaying the density $\rho = \frac{B_0^2\beta}{4\pi g\Lambda_0} D_{KS}(Y)$, vertical field-component $B_z = B_0 h_{KS}(Y)$ and field-line curve $Z = Z_{KS}(Y)$, given by Equations (44)-(47).

Displayed in Figure 4 is the solution with the physical variables,

$$B_z = B_0 \tanh\frac{\sqrt{\beta}}{2}Y, \tag{44}$$

$$p = \frac{B_0^2}{8\pi}\beta \operatorname{sech}^2\frac{\sqrt{\beta}}{2}Y, \tag{45}$$

$$\rho = \frac{B_0^2}{8\pi g}\frac{\beta}{\Lambda_0} \operatorname{sech}^2\frac{\sqrt{\beta}}{2}Y, \tag{46}$$

$$Z = Z_0 + 2\log\cosh\frac{\sqrt{\beta}}{2}Y. \tag{47}$$

The field line (47) is identified by its intersection point $(0, Z_0)$ on the Y axis. The KS-slab has the simple mass function

$$m_{KS}(h) = h, \tag{48}$$

obtained by setting $\mu_1 = 0$ in Equation (39), or, alternatively, by direct calculation using Equation (37).

The parameter Λ_0 is a measure of *vertical* gravitational stratification. The Y-variation in this 1D slab is a manifestation of stratification along identical, geometrically-2D field lines

described by Equation (47) in the (Y, Z) plane. Rewrite this equation as

$$\exp\left[-\left(Z - Z_0\right)\right] = \mathrm{sech}^2 \frac{\sqrt{\beta}}{2} Y, \tag{49}$$

and Equations (45) and (46) show that the Y-variations of the pressure and density correspond to an exponential decrease with Z along a field line of constant Z_0. The Lorentz force has no component along the field and in that direction the pressure-gradient force alone supports the weight of the isothermal fluid with a scale height Λ_0 just as seen in a plane-parallel isothermal atmosphere. The isothermal atmosphere has an infinite extension, i.e., the top of the atmosphere defined by $p = 0$ is located at infinity up every field line. This top of atmosphere locates the boundaries of the Y-varying slab at infinity, i.e., $Y = \pm Y_1 \to \pm\infty$.

The KS slab has a simple generalization[2] if $\eta \neq 0$ and $\mu = 0$ with $\mu_1 = 0$. We recover the algebraic equation (42) giving $u(h)$. With $\eta \neq 0$, the resistive velocity $v(h)$ is nonzero, given explicitly by Equation (21). Therefore this inviscid slab falls resistively across the field but has the same density and field distributions as the static KS slab.

Not every static atmosphere extends to infinity. The polytropic plane-parallel atmosphere is an instructive example of an atmosphere with its top $p = 0$ continuing into vacuum at a finite height[37,38]. The temperature is a function of the density, $T \propto \rho^{\gamma-1}$, γ being the polytropic index. In the decline of pressure and density with height, the spatially-variable scale height $\Lambda_0 \propto T$ decreases with both density and pressure zero at a finite height. We shall see that the presence of a viscous flow has the same effect of terminating an atmosphere at a finite height.

2. The $\mu_1 = 2.0$ resistive-viscous slab

Fig. 5 displays a representative BVP-solution $u(h)$ for a resistive-viscous slab with $\beta = 1.0, \mu_1 = 2.0$, the one labelled (v) among the trial solutions in the left panel of Fig. 2. In the Runge-Kutta computation carried out, we solved the equivalent BVP posed for $q = u^2$ by ODE (32) and boundary conditions (33) and then define $u(h) = q^{1/2}$. The computed $q(h)$ is displayed as a dashed curve in Fig. 5. With $u(h)$ known, its gradient determines the mass function $m(h)$ given by Equation (39). Also shown is the density $D(h)$ explicitly given in terms of h by Equation (20).

The numerical solution $Y(h)$ to ODE (35) transforms the BVP-solution in h-space into

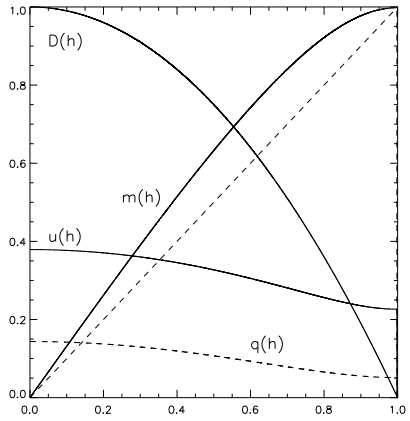

FIG. 5. A global solution of the current-density u as a function of h on the abscissa, with $\mu_1 = 2.0$. The mass function $m(h)$ and density $D(h)$, together with $q(h) = u^2$ as a dashed graph, are displayed.

the physical variables as functions of Y shown in Fig. 6, separately displaying the fluid and field properties on the left and right panels, respectively. All properties are suitably scaled to fit into the sub-figures. Consistent with $u \neq 0$ at $h = 1$ in Fig. 5, the integral (36) gives $Y_1 = 3.25$ approximately. The density decreases from a maximum at slab center to zero at slab boundary $Y = Y_1$ beyond which is vacuum. The downward resistive velocity $v(Y)$ and the current density $u(Y)$, flowing in the x direction, are proportional in amplitude. Their amplitudes decrease outward from maximum at slab center to drop discontinuously to zero across the boundary $Y = Y_1$ with vacuum. The representative field line is parabolic in shape due to a uniform $B_y = B_0$ superposed with a $B_z = B_0\beta^{1/2}h(Y)$ increasing monotonically from zero at slab center to the value $B_z = B_0\beta^{1/2}$ at slab boundary $Y = Y_1$ with $h(Y_1) = 1$. This slab field continues into the $Y > Y_1$ vacuum as the uniform field $\mathbf{B}_0 = B_0\left(1, \beta^{1/2}\right)$ fixed at $Y = Y_1$.

The fluid and field distributions of the equal-M_T KS slab are plotted in dashed curves in Fig. 6 for comparison with the $\mu_1 = 2.0$ resistive-viscous slab. The static KS slab extends out to infinity with a current-density everywhere nonzero to give rise to an everywhere-vertical tension force as the only means to support the weight of the fluid. By artificially introducing resistivity and viscosity into the KS slab as an initial state will result in a time-dependent, resistive-viscous flow collapsing the slab inward. As the motions generated escape as MHD waves to infinity in the unbounded space, the slab may seek a finite-width

slab represented by the $\mu_1 = 2.0$ solution as an end state. This possible scenario involves a complete withdrawal of the fluid in the KS slab from infinity to relocate the slab boundaries at finite distances. Viscosity plays an essential role.

The role of viscosity in structuring the $\mu_1 = 2.0$ slab is in full evidence in Figs. 5 and 6. The gradient of the (normalized) downward flow $V(Y)$ increases from zero at $Y = 0$ to a maximum value at an intermediate point, denoted by $Y = Y_{max}$, and then decreases to zero at $Y = Y_1$. The viscous force is everywhere vertical and proportional to the second derivative of $V(Y)$; see Equation (9), so the viscous force is upward in $0 < Y < Y_{max}$ providing a means of supporting the weight of the fluid. As the density profiles of the two equal-M_T slabs show in Fig. 6, the sweeping of same total linear mass M_T into the finite-width, resistive-viscous slab involves a significant viscous force to support the main weight around the slab center. So strong is the upward viscous force in this locality that the field is less dipped, and the tension force weaker, than seen in the field of the KS slab; that is, for the same $B_y = B_0$, the vertical field component is stronger in the KS slab than the resistive-viscous slab. Since no frictional force can be borne upon vacuum, the uplifting by the upward viscous force in $0 < Y < Y_{max}$ involves a reacting downward viscous force on the outer layer of the slab, represented by the negative second derivative of $V(Y)$ in the layer $Y_{max} < Y < Y_1$. The magnetic field must then be dipped just right to provide a tension force that balances the downward viscous force as well as the weight of the fluid in this outer layer.

The first derivative of $V(Y)$ at a point Y gives the net viscous force acting on the fluid layer from slab center to that point. The mass function $m(Y)$ is the linear total mass in this layer as a fraction of M_T. Thus, this net viscous force is maximum if $Y = Y_{max}$ and reduces to zero if $Y = Y_1$, the latter indicating zero frictional bearing on vacuum. This distribution of the net viscous force explains the difference in mass functions $m - m_{KS} \geq 0$ between the two slabs shown in Figs. 5 and 6. The vanishing of the that difference at $Y = Y_1$, i.e., $h = 1$, indicates that the net viscous force for the entire resistive-viscous slab is zero, and the weight of the total linear mass M_T is entirely magnetically supported in both the KS slab and the resistive-viscous slabs.

The direct influence of viscosity on the width of the slab may be seen in terms of an apparent density scale height along each field line in the $Y - Z$ plane. The Lorentz force has no component along the field line, requiring the isothermal pressure to balance both viscous and gravitational forces in the field-aligned direction. An upward viscous force reduces the

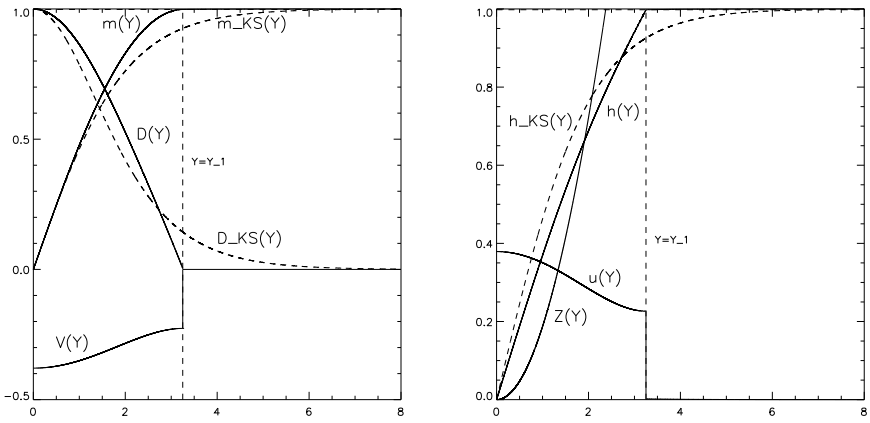

FIG. 6. The $\mu_1 = 2.0$ resistive-viscous slab in physical space, of a finite-width $2Y_1 \approx 7$, falling with dimensionless velocity $V(Y) = -u(Y)$ shown in the left panel, where $u(Y)$ is the current density shown in the right panel. The density $D(Y)$ monotonically decreases to zero at $|Y| = Y_1$, remaining zero in $|Y| > Y_1$; to be compared with the (dashed) static KS density $D_{KS}(Y)$. The mass functions $m(Y)$ and (dashed) $m_{KS}(Y)$ confirm that both slabs have the same total mass. The vertical field-component $h(Y)$ monotonically increases to its maximum value at $|Y| = Y_1$ and stays at that value for $|Y| > Y_1$. Its gradient gives the current-density $u(Y)$ shown, nonzero in the slab and discontinuously dropping to zero across $|Y| = Y_1$ into vacuum. The representative field line $Z = Z(Y)$ shown has a parabolic shape, exiting the slab at a vertical point on $|Y| = Y_1$ outside the range of the graphs, beyond which the field line is straight at a fixed incline to the vertical. The (dashed) KS vertical field-component $h_{KS}(Y)$ is plotted for comparison.

pull of gravity and the pressure supports a lightened fluid by declining with height along the field more gradually than at rate of the hydrostatic scale height Λ_0. This is the case around the slab center, $0 < Y < Y_{max}$. Whereas, in the outer layer, $Y_{max} < Y < Y_1$, a downward viscous force enhances the pull of gravity, requiring a pressure declining along the field more steeply than hydrostatic to support the enhanced weight. If this pressure decline is sufficiently steep as determined by the nonlinear equations, the pressure and density decrease to zero at a finite height along the field line to produce the finite width of the slab in Fig. 6.

E. The $0 < \mu_1 < \mu_c$ resistive-viscous slabs

In Sub-section (II C), the numerical solutions $u(h)$ to ODE (29) presented for $\mu_1 = 2.0, 0.4, 0.1, 0.066$ are sufficient to demonstrate the existence of a critical parameter $0.1 < \mu_c < 0.4$ associated with the following property. The BVP (29) and (34) has a solution only if $\mu_1 > \mu_c$. Note that μ_1 is the only free (dimensionless) parameter in ODE (29), whereas the additional prescription of $\beta = 1$ is needed only for constructing field and fluid distributions out of the solution $u(h)$. In the regime $0 < \mu_1 < \mu_c$, BVP (29) and (34) has no solution if $u \neq 0$ at end point $h = 1$. Demanding for $u = du/dh = 0$ at $h = 1$ is an over-specification, mathematically not admissible. Boundary conditions (34) are derived from the boundary conditions (31) in the transformation of the FBP in Y-space into the BVP in h-space under the assumption that u is positive definite. Therefore we return to the original boundary conditions (31) that set $du^2/dh = 0$ at end-point $h = 1$ in order that no viscous force is exerted on vacuum. It thus follows that in the regime $0 < \mu_1 < \mu_c$ the physical FBP corresponds to a different BVP, henceforth referred to as the revised BVP, posed by ODE (29) subject to the boundary conditions,

$$h = 0, \quad \frac{du}{dh} = 0, \tag{50}$$

$$h = 1, \quad u = 0, \tag{51}$$

where we demand for u to vanish, instead of du/dh, at end-point $h = 1$. In this case the end-point is a singularity point of ODE (29), complicating the BVP we need to solve. This mathematical complication is treated in Appendix A based upon which we focus on demonstrating below that the revised BVP has solutions only for a possibly infinite set Ω of discrete values of μ_1 in the range $0 < \mu_1 < \mu_c$.

In an infinitesimally small neighborhood of $h = 1$, there are two independent local solutions that vanish at $h = 1$. One of them is a one-parameter solution related to the trial solutions $u(h)$ in Figs. 2 and 3 that vanish at an interior point $h = h_1 < 1$. Treating h_1 as a varying parameter, these solutions define a limit local solution around $h = 1$ as $h_1 \to 1$. As shown in the Appendix A, such a limit solution u vanishes as $(1 - h)^{1/2}$ at $h = 1$ with an unbounded gradient; see Figs. 2 and 3. In this case, $du^2/dh \neq 0$ in violation of boundary conditions (31).

The other independent local solution,

$$u_L(\epsilon) = \sum_{n=1}^{\infty} a_n \epsilon^n, \tag{52}$$

as a Taylor expansion in $\epsilon = 1 - h_1 > 0$ with constant coefficients a_n is the only possibility for a solution to the revised BVP. This solution vanishing at $h = 1$ with $du/dh = -a_1$ meets the viscosity condition $du^2/dh = 0$ at $h = 1$. Transform ODE (29) into the form

$$\mu_1 u \frac{d^2u^2}{d\epsilon^2} - 2u + 2\epsilon - \epsilon^2 = 0, \tag{53}$$

with $\epsilon = 1 - h_1 > 0$. Then substituting $u = u_L(\epsilon)$ generates a set of nonlinear algebraic recursive equations to determine the coefficients a_n. The nature of the singularity point at $h = 1$ is that solution $u_L(\epsilon)$ is a particular solution with no free parameter. Assuming a finite radius of convergence for the series (52), the recursive equations determine all the a_n coefficients in terms of μ_1. In particular, a_1 is a root of the cublic equation (A14) which we rewrite in the form

$$\mu_1 = \frac{a_1 - 1}{a_1^3}, \tag{54}$$

for our purpose here. The task in this investigation is then to determine whether for each given value in the range $0 < \mu_1 < \mu_c$, the uniquely-determined local solution $u_L(\epsilon)$ exists. If it does exist, can $u_L(\epsilon)$ be extrapolated from $\epsilon = 0$ to $\epsilon = 1$, i.e., from $h = 1$ back to $h = 0$ to satisfy the symmetry condition $du/dh = 0$ at $h = 0$, demanded by boundary conditions (51)? Our computational construction of global solutions to the revised BVP suggests that most values in the range $0 < \mu_1 < \mu_c$ do not admit a global solution. These computations are summarized below.

1. The local solution $u = u_L(\epsilon)$

Equation (54) expresses μ_1 strictly in terms of the gradient $du/dh = a_1$ at $h = 1$. We may therefore generate the particular solution $u_L(\epsilon)$ using a_1 as a free parameter in terms of which μ_1 and the other coefficients $a_n,\ n = 2, 3, 4, ...$ are defined. By definition μ_1 is positive, requiring $a_1 > 1$ in Equation (54). Fig. 7 is a graph of $\mu_1(a_1)$, showing that the admissible range $a_1 > 1$ generates a limited range $0 < \mu_1 \leq \mu_1^{max} = 4/27$. In this range, each μ_1 is associated with two a_1-roots of cubic equation (A14), an inner one in $1 < a_1 < 3/2$ and an outer one in $3/2 < a_1 < \infty$. The two roots coincide at $a_1 = 3/2$ when $\mu_1 = \mu_1^{max}$. The two

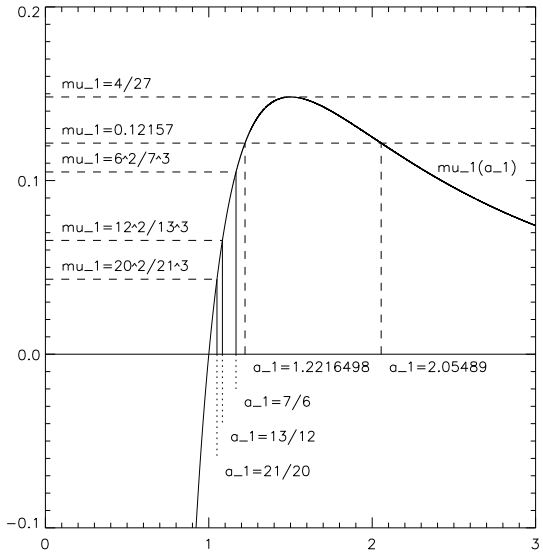

FIG. 7. The function $\mu_1(a_1)$ displaying the maximum value $4/27$, the two values $a_1 = 1.2216498, 2.05489$ on the abscissa giving $\mu_1 = 0.12157$, and the first three points of the infinite sequences $\mathcal{M}$ and $\mathcal{A}_I$ described in the text.

roots generate two separate branches of the local solutions $u(h) = u_L^{(\mp)}(a_1, \epsilon)$, modifying our notation with the superscripts $\mp$ to identify with the inner and outer a_1-roots associated with a given μ_1. Hereafter, if the $\mp$ superscripts are not displayed, we mean both branches of the solution for a given μ_1. In Fig. 7 the illustrative case of $\mu_1 = 0.12157$ having the two roots $a_1 = 1.2216498, 2.05489$, given to high numerical precision, will take on a physical significance later in our analysis.

Direct calculation gives

$$u_L(\epsilon) = a_1\epsilon\left[1 + \frac{1}{2(6a_1-7)}\epsilon - \frac{3(a_1-1)}{(12a_1-13)(6a_1-7)^2}\epsilon^2 + \frac{(a_1-1)(192a_1-189)}{4(20a_1-21)(12a_1-13)(6a_1-7)^3}\epsilon^3 + ...\right], \quad (55)$$

using Equation (54) to express μ_1 in terms of a_1. The coefficients a_n for $n \geq 2$ as functions of a_1 all have poles, the first 3 poles in evidence in series (55). To identify all these poles, we first note from the general derivation for an order $N \geq 2$ that each coefficient a_N as a function of a_1 diverges at the point $a_1 = R_I(N)$ where

$$R_I(N) = \frac{N^2+N+1}{N^2+N}. \quad (56)$$

Moreover, at $a_1 = R_I(N)$, all coefficients a_n of order $n > N$ also diverge whereas all coefficients a_n of order $n < N$ are finite. In series (55), we specifically have: $R_I(2) = 7/6, R_I(3) = 13/12, R_I(4) = 21/20$. Equation (54) gives the μ_1-value for each $a_1 = R_I(N)$:

$$\mu_1^{(N)} = \frac{(N^2+N)^2}{(N^2+N+1)^3}. \tag{57}$$

Substituting $\mu_1 = \mu_1^{(N)}$ into cubic equation (A14) naturally recovers $a_1 = R_I(N)$ as one of the three roots, the other two roots being

$$R_{II}(N) = \frac{N^2+N+1}{N+1}, \tag{58}$$

$$R_{III}(N) = -\frac{N^2+N+1}{N}. \tag{59}$$

The third root $R_{III}(N)$ has no interest since it gives an unphysical negative μ_1. The second root $R_{II}(N)$ corresponds with $R_I(N)$ as the outer and inner positive a_1-roots for each $\mu_1 = \mu_1^{(N)}$.

To summarize the mathematical results, let $\mathcal{A}_I \equiv [R_I(N)]_{N=2,3,4,...}$ denote the monotonically decreasing sequence of the poles $a_1 = R_I(N)$ of the constant coefficients a_n in series (55) defining local solution $u_L(\epsilon)$, with $R_I(N) \to 0$ as $N \to \infty$. This infinite sequence defines the corresponding monotonically increasing sequence $\mathcal{A}_{II} \equiv [R_{II}(N)]_{N=2,3,4,...}$, with $R_{II}(N) \to \infty$ as $N \to \infty$. For $N = 2, 3, 4, ...$, the pair $[R_I(N), R_{II}(N)]$ from sequences $\mathcal{A}_I$ and $\mathcal{A}_{II}$ are the inner and outer a_1-roots giving the same value of $\mu_1 = \mu_1^{(N)}$ by Equation (54). So we define the monotonically decreasing sequence $\mathcal{M} \equiv \left[\mu_1^{(N)}\right]_{N=2,3,4,...}$ that starts from $\mu_1^{(2)} = 6^2/7^3 \approx 0.1045$ and converges to $\mu_1^{(\infty)} = 0.0$ as an accumulation point.

The physical significance of these results is that if we are given μ_1 and $\mu_1 \in \mathcal{M}$, the local solution $u_L^-(\epsilon)$, corresponding to the inner root $a_1 \in \mathcal{A}_I$ definitely does not exist because the expansion coefficients a_n are not bounded. Then, there is only one local solution $u_L^+(\epsilon)$ corresponding to the outer root $a_1 \in \mathcal{A}_{II}$ assuming that the corresponding series (55) is convergent. From continuity argument, we may assume that as a function of parameter a_1, the local solution $u_L^-(\epsilon)$ does not exist in an open interval centered at each inner root $a_1 \in \mathcal{A}_I$. That is, in μ_1-space, there is a corresponding open interval centered at each $\mu_1 \in \mathcal{M}$ where, at most, only one local solution may exist, namely, $u_L^-(\epsilon)$. Prepared with these analytical properties, we are able to establish the following numerically demonstrated results on the steady states available to the resistive-viscous fluid in the range $0 < \mu_1 < \mu_c$.

2. Numerical solutions to the revised BVP

Consider the solution to the BVP in h-space as a function of a_1 in the open interval $(1, \infty)$ in Fig. 7. The coefficients a_n in the series (55) giving the local solution $u_L(\epsilon)$ are free of poles for all n in the open subinterval $[R_I(2), \infty] = (7/6, \infty)$. Being free of poles is not a sufficient condition for the series (55) to be convergent. We avoid the formidable task of proving convergence and adopt the following numerical approach to our problem. We take the series (55) to the fourth order in ϵ to formally define $u_L(\epsilon)$ in an empirically determined small neighborhood of end point $h = 1$. Then we use a Runge-Kutta solver to numerically integrate from $u_L(\epsilon)$ at a point in that neighborhood inward to arrive at $h = 0$. If the globally computed solution yields a u^2 numerically determined to have zero derivative at $h = 0$, we would have demonstrated that a global solution to the BVP exists for the particular value of a_1 used in computation, and, therefore, for the particular value of μ_1 determined by the a_1-value used.

Figure 8 presents a sample set of solutions $u(h)$ numerically integrated inward from near $h = 1$ for $a_1 = 1.2216498, 3/2, 7/3, 13/4, 21/5$. These and other numerical solutions, not presented in Figure 8, for many other values of a_1 in the open interval $[R_I(2), \infty] = (7/6, \infty)$ show a smooth solution $u(h)$ emerging from near $h = 1$ for each prescribed a_1. For $3/2 \leq a_1$, the shape of the computed $u(h)$ depends on a_1 continuously. All these computed $u(h)$ increase monotonically as h decreases from near $h = 1$ to go out of computational range without arriving at $h = 0$. We conclude from this demonstration that there are no global solutions in the range $3/2 \leq a_1$. The numerical solutions for $a_1 = 3/2, 7/3, 13/4, 21/5$ displayed in Figure 8 are representative.

The three cases of a_1 with values $[R_{II}(2), R_{II}(3), R_{II}(4)] \equiv (7/3, 13/4, 21/5)$ are particularly significant. These are the outer a_1-roots of $\mu_1 = [\mu_1^{(2)}, \mu_1^{(3)}, \mu_1^{(4)}] \equiv (6^2/7^3, 12^2/13^3, 20^2/21^3)$, respectively, and each of them admits no 1D steady states. The local solution $u_L(\epsilon)$ exists in each of these three cases, but the global solution meeting the boundary condition at $h = 0$ does not exist. Now, we also know that the global solution does not exist for $a_1 = [R_I(2), R_I(3), R_I(4)] \equiv (7/6, 13/12, 21/20)$, the respective inner a_1-roots of the preceding three values $\mu_1 \in \mathcal{M}$. In each case, the local solution $u_L(\epsilon)$ does not even exist since an infinite number of its coefficients a_n are unbounded. Therefore, we have the numerically demonstrated conclusion that all the μ_1-values in $\mathcal{M}$ admit no global solutions to

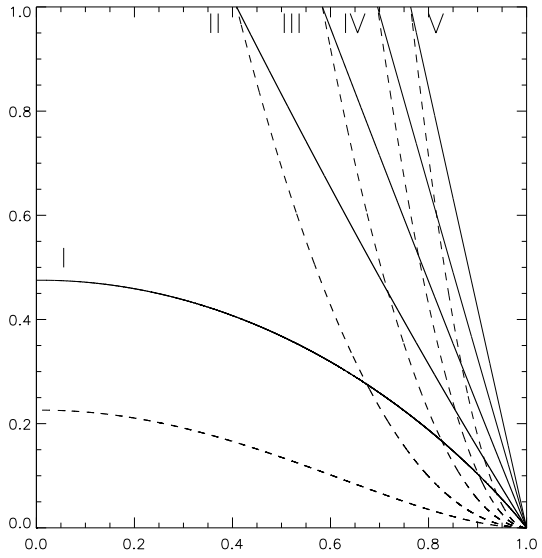

FIG. 8. Numerical solutions of current-density u as functions of h on the abscissa, each integrated from the local solution $u_L(a_1, h)$ given by series (55), starting from a small neighborhood of end point $h = 1$ towards $h = 0$, for (I) $a_1 = 1.2216498$, (II) $a_1 = 3/2$, (III) $a_1 = 7/3$, (IV) $a_1 = 13/4$, (V) $a_1 = 21/5$ as labelled. Each numerical solution u is displayed as a solid graph accompanied by a dashed graph for $q = u^2$. As described in the text, solution (I) is a proper global solution to the BVP for $u(h)$, whereas the other four solutions monotonically increase as h decreases from $h = 1$ without arriving with zero gradient at $h = 0$.

the BVP, and, hence, no solution to the FBP for the resistive-viscous slab. In other words the states $\mu_1 \in \mathcal{M}$ must be either a permanently time-dependent 1 D state or a state of multi-dimensional spatial variations. Moreover, the series (55) fails to converge not just at each pole of the series coefficients a_n but also, at least, in an infinitesimal neighborhood of the pole. Hence, no 1D steady states can be found in the infinitesimal μ_1-neighborhoods around each of the $\mu_1 \in \mathcal{M}$.

Figure 8 shows that the numerical solution evolving continuously with a_1 becomes sensitive to a_1 as the critical value $a_1 = R_I(2) = 7/6$ is approached from above. The first global solution with $a_1 \approx 1.2216498, \mu_1 \approx 0.12157$ is encountered as shown. As a_1 decreases below that of the global solution, no solution is found all the way past $a_1 = R_I(2) = 7/6$ and further on past $a_1 = R_I(3) = 23/12$, that is, there are no global solution in the range

$R_I(3) < a_1 < R_I(2)$.

The first global solution $u(h)$ with $a_1 \approx 1.2216498, \mu_1 \approx 0.12157$ is displayed in Figure 9 with its transformation into the fluid and field variables of the resistive-viscous slab. In the left panel the numerical solutions $u(h)$ for three values $a_1 = 1.2216, 1.2216498, 1.2217$ are shown. The $a_1 = 1.2216498$ global solution meets the boundary condition of zero u^2-gradient at $h = 0$, whereas the other two numerical solutions with a_1-values just above and below fail to meet this boundary condition at $h = 0$. Within computational accuracy, the global solution obtains only for $a_1 = 1.2216498, \mu_1 = 0.12157$ as an isolated point in a_1-space, or, equivalently, in μ_1-space. For this global solution, $u(h) \approx a_1\epsilon$ as $\epsilon \to 0$ at $h = 1$, the integral (36) diverges logarithmically, i.e., $Y_1 = \infty$, and we have a slab of infinite width, like the static KS slab, as shown in the right panel. For comparison the density $D_{KS}(Y)$ and vertical field-component $h_{KS}(Y)$ of the static KS slab with the same total mass are plotted as dashed graphs, showing a weak departure between the two dynamically different slabs, except that one has a resistive-viscous flow and the other is absolutely static. Our numerical search for a global solution to the BVP discovered a second one with $a_1 = 1.08102875, \mu_1 = 0.064$ in the range $R_I(4) = 1.050 < a_1 < R_I(3) = 1.083$. This global solution also has a weak departure from the static KS slab. The global solution initiated from $u_L(a_1, h)$ from a small neighborhood of $h = 1$ depends on a_1 with extreme sensitivity in $a_1 < 3/2$.

Before proceeding, a few remarks on the computations are in order. Our search for global solutions with $a_1 < R_I(4)$ encountered computational difficulties in dealing with the required high spatial-resolutions and capability to resolve densely-spaced discrete eigenvalues[39,40]. For numerical accuracy and stability, the Runge-Kutta method applied to nonlinear ODE (32) subjects the grid spacing Δh of the independent variable to uncompromising upper and lower bounds, thus putting a severe constraint on numerical resolution. The high-precision numbers in the caption of Fig. 9 indicate the delicate treatments of these computational difficulties. For example, a small change in a_1, from $a_1 \approx 1.2216498$ to $a_1 \approx 1.08102875$, incurs a large change to the global solution.

The revised BVP is a nonlinear problem but it has a basic feature of the linear eigenfunction theory. Each value in the range $\mu_1 > \mu_c$ admits global solutions, so μ_1 behaves like a continuous eigenvalue in this range. For $\mu_1 < \mu_c$, global solutions appear to exist only for point values of μ_1, corresponding to the usual discrete eigenvalues. These nonlinear equivalents of discrete eigenvalues are separated by open μ_1-intervals centered around each

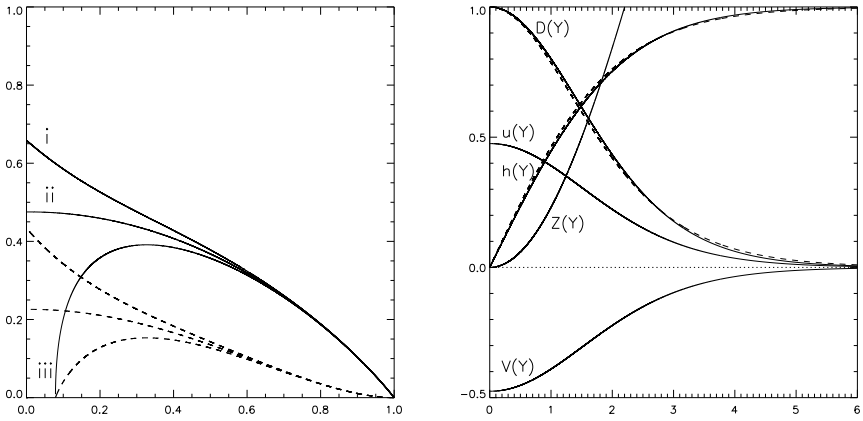

FIG. 9. Numerical solution I in Figure 8, generated by $a_1 = 1.2216498$ located in the open interval $(R_1(2), 3/2) \equiv (7/6, 3/2)$ as a proper global solution to the BVP for $u(h)$ with $\mu_1 = 0.12157$. In the left panel this numerical solution $u(h)$ is shown with two other numerical solutions of nearby a_1-values, namely, $a_1 = 1.2216000, 1.2217000$, to demonstrate that to numerical accuracy the global solution exists as a solution of the BVP only at the isolated value $a_1 = 1.2216498$ corresponding to $\mu_1 = 0.12157$. The resistive-viscous slab in physical space corresponding to this global solution extends to infinity in both directions, shown in solid graphs for $D(Y)$, $u(Y)$, $H(Y)$ and $Z(Y)$ in the right panel. These distributions are in small departures from the corresponding quantities in dashed graphs for the static Kippenhahn-Schlüter with the same temperature and total mass.

$\mu_1 \in \mathcal{M}$. Moreover, both separations and the width of these μ_1-intervals are vanishingly small for index $N \to \infty$. For our purpose in this paper, let us conjecture that discrete eigenvalues exist in an infinite number of open intervals $(R_I(N+1), R_I(N))$. This conjecture seems a reasonable working hypothesis, since we have shown that, at least, two eigenvalues exist; see Figures 8 and 9, and we also know that $\mu_1 = 0$ is an eigenvalue associated with two steady states, the static KS slab with $\eta = 0$ and its generalization allowing for an inviscid-resistive flow.

Let us then denote the set of conjectured point-eigenvalues by $\Omega = \omega(i), i = 1, 2, 3, ...$ where $\omega(1) = 0.12157, \omega(2) = 0.064, ...\omega(\infty) = 0.0$. The existence of this discrete spectrum has two implications. Zweibel[41] has shown that the static KS slab is stable to infinitesimal perturbation assuming $\eta = \mu = 0$. This MHD stability analysis should be extended to the

second KS resistive-inviscid slab as well as the unbounded number of $\omega(N) \to 0$ eigenstates densely populated around the limit $\mu_1 = 0$. How does the existence of these steady states as discrete points in μ_1-space manifest in the stability of each admissible eigenstate in Ω?

The infinite number of steady states with $\mu_1 \in \Omega$ are densely distributed as discrete-points around $\mu_1 = 0$ as an accumulation point. The set Ω is of measure zero compared to its complement set $\mathcal{M}$ containing μ_1-values admitting no 1D steady states. Therefore the set Ω, densely distributed around $\mu_1 = 0$ within itself, by that measure is sparsely distributed amidst the μ_1-values of $\mathcal{M}$. This topological structure of 1D steady states, being sparsely separated by a profusion of necessarily time-dependent or multi-dimensional states, is similar to that associated with the onset of hydrodynamic turbulence as the Reynolds number is increased beyond a critical number, described in Chapter III of the book[3] by Landau & Liftshitz. This picture also suggests that a critical number $\mu_1^T < \mu_1^{max}$ exists such that all slabs with $\mu_1 < \mu_1^T$ are necessarily turbulent. The energy liberated by the falling slab is an inexhaustible source for driving the expected turbulence.

III. SUMMARY AND CONCLUSION

This is a basic study of a complex nonlinear MHD process, the resistive flow of a compressible viscous fluid, under its own weight, across a dipped magnetic field. The process can be greatly complicated by its coupling with thermodynamics and energy transport, such as believed to be taking place in the interior of the solar prominence shown in Figure 1[2,8,10,42]. Our study has a limited scope, investigating the steady states available to the 1D mathematical system describing an infinite slab in unbounded space, taking the two coefficients, μ and η for viscosity and resistivity, respectively, to be uniform in space. The aforementioned thermal coupling is avoided by assuming the isothermal condition under the ideal gas law. Despite the simplifications, this 1D system presents a challenging free-boundary problem.

Compressibility is a central effect in the interplay among the Lorentz, viscous, fluid-pressure, and gravitational forces that structures the fluid slab and its downward resistive flow. Force balance is coupled to the unknown locations of the free-boundaries $Y = \pm Y_1$ where $D(\pm Y_1) = 0$ in the symmetric slab studied. If Y_1 is finite, the field $\mathbf{B}$ in the slab extends as oppositely-inclined uniform fields in the two external vacuum regions. If Y_1 is infinite, the non-potential field, resistive flow and density of the slab extend all the way

in either directions to infinity where $D \to 0$. The tractability of our study comes from decoupling the unknown Y_1 from the fluid and field structures to be constructed. Cleanly transforming the FBP in Y-space into a numerically tractable BVP for the dimensionless current-density $u(h)$ in h-space permits the fluid and velocity structures to be constructed independent of Y_1; h being the dimensionless form of $B_z(y)$. Based on the solution $u(h)$ obtained, the explicit form of $h(Y)$ and the value Y_1 are self-consistently determined by the final separate step of calculation.

In physical terms, the FBP seeks the steady state of a slab of a given linear total mass M_T that has deformed a horizontal field $\mathbf{B}_{initial} = B_0\hat{y}$ into the dipped field $\mathbf{B} = B_0\,[\hat{y} + H(y)\hat{z}]$, such that a vertical steady flow is maintained via a balance among the four forces. Each physical realization of the 1D system is specified by its invariants $(M_T, g, \eta, \mu, \Lambda_0, B_0)$. The solution to the BVP for $u(h)$ describes the steady state we seek and this solution carries just one free parameter, the dimensionless constant μ_1 given by Equation (30) in terms of the system invariants. Essentially, μ_1 is proportional to the triple product $\eta\mu M_T^2$. Our numerical solutions indicate that for $\mu_1 > \mu_c$ the solution to the FBP exists and varies continuously with μ_1, where μ_c is a computable bound of the order of $\mu_1^{max} = 4/27$. Each of these solutions describes a steadily descending slab of a finite μ_1-dependent width.

Consider a fluid of a finite M_T extending to great distances in both directions in y, not in equilibrium in an initial field $\mathbf{B}_{initial} = B_0\hat{y}$. The invariants $(M_T, g, \eta, \mu, \Lambda_0, B_0)$ as well as μ_1 of this system are fixed by the initial state and preserved during the evolution of the fluid. This fluid will collapse into a steadily descending slab of a finite width determined by the invariant μ_1. Viscosity is essential to the the slab's collapse into a finite width. This process is a version of the magneto-gravitation collapse of interstellar clouds proposed by Parker[32–35].

The general non-existence of a steady state in the regime $\mu_1 < \mu_c$ is intriguing. Our numerical solutions show that steady states exist in this regime only for discrete values of $\mu_1 \in \Omega$. We thus have a nonlinear analogy of the familiar linear eigenfunction theory. In our problem, μ_1 is a nonlinear eigenvalue that takes a continuous form in $\mu_1 > \mu_c$ and a discrete form in $\mu_1 < \mu_c$. In the notations in Subsection II E, our numerical search for $u(h)$ solutions to the BVP suggests that the discrete spectrum Ω of eigenvalues is infinite. We are able to locate the first two eigenvalues, $\omega(1) = 0.12157, \omega(2) = 0.064$, with eigenfunction $u(h)$; see Figs. 8 and 9. Accepting that there is an infinity of discrete eigenvalues in Ω, we may then

identify $\omega(\infty) = \mu_1 = 0$ with the static KS slab and its generalization to include an inviscid resistive flow. Like the $\mu_1 = 0$ states, all the eigenstates in Ω describe a slab with infinite width, that is, density and flow extend in both directions in y to infinity where the density is vanishingly small.

The exact analytical results of Subsection II E, supported by numerical evidence, is certain that an uncountably infinitely large set of $\mu_1 < \mu_c$ do not admit 1D steady states. In particular, all values of μ_1 in an infinitesimal μ_1-neighborhood centered around each point $\mu_1 \in \mathcal{M}$, corresponding to $a_1 \in A_I \equiv [R_I(N), N = 2, 3, 4, ...]$, do not admit 1D steady states. Since μ_1 is an invariant fixed for each specific 1D system, we have the result that when no 1D steady state is available, the system must be permanently time-dependent or be in a steady state with multi-dimensional spatial variations[26,43–45]. The former implication may take the form of a nonlinearly oscillatory descent of the slab across the field that generates MHD waves traveling out to infinity. Gravity is the source of the energy dissipated in situ by resistivity and viscosity as well as the wave energy carried steadily away from the descending slab. The latter implication may take the form of 2D or 3D steady states, an example suggested in the Appendix B.

Accepting the conjecture that Ω is an infinite set, perhaps a countable set as we have assumed, we have the rich topological structure of the dense intermingling of presence and absence of the 1D steady states in μ_1-space described in Subsection II E. This topological structure is similar to that described by Landau & Liftshitz[3] to explain the onset of hydrodynamic turbulence. In the latter, a dense intermingling of states of laminar flow and states of time-dependent evolution is encountered in phase space as the inverse Reynolds number R^{-1} decreases and falls below a critical value R_{crit}^{-1}. The laminar flows are highly unstable in this topological structure of physical states and crossing that critical value ushers in turbulence as the preferred state, assuming that there is a source energy to sustain the turbulence. In that similarity, we have a basis to expect that $\mu_1 \to 0$ contains a critical number μ_{crit}, conceptually corresponding to the critical value of R_{crit}^{-1}, such that for $\mu_1 < \mu_{crit}$, turbulence is the preferred state of the slab. The gravitational potential energy liberated by the fall of the slab is a ready source of energy to drive such a turbulence. Therefore, it is important in future work to confirm or refute that the set Ω is infinite, with the possibility of Ω containing structures more complex than we envisage in our numerical study. Zweibel[41] has shown that under the condition of $\eta = \mu = 0$, the static KS slab is, at worst, marginally stable in

response to linear perturbations. This seminal study should be extended to the steady 1D slabs wherever they are admitted in the regime $\mu_1 \to 0$ under the action of double-diffusion with non-zero η and μ. We expect that the dense inter-minging of steady and unsteady states implied by our study must manifest in the linear-stability properties.

Idealizing the solar coronal plasma to be fully ionized hydrogen at a million-degree temperature, the estimated coefficients of resistivity and viscosity are such that typically $\mu_1 << 1$, suggesting the relevance of the $\mu_1 \to 0$ regime of our 1D slab model. The expectation that this regime is necessarily turbulent is a possible explanation of the turbulence recently observed with unprecedented resolutions by space instruments[13,17]. The magneto-gravitational collapse of the fluid as well as the viscous collimation of the downward fluid to a finite width may also be relevant if we accept the conclusion[2,26] that coronal plasmas are more resistive than indicated by their small molecular resistivity. Parker[27–31,43,45] concluded on theoretical ground that under conditions of extremely high electrical conductivity in the corona, the frozen-in fields tend to form tangential discontinuities that carry extremely thin current sheets. The electrical conductivity is high but not infinite. Thus the current sheets must dissipate when, by the action of MHD forces, they have thinned below a threshold at which the weak resistivity becomes physically significant. Current dissipation then takes place with magnetic reconnection[46]. These effects are multi-dimensional. Thus we may interpret our 1D model with its collimation of narrow resistive flow to represents the corona with a resistivity enhanced by small-scale current-sheet formation and dissipation.

These implications for the observed prominence have motivated our simple study where we concentrated on understanding the novel elementary MHD properties exhibited in the 1D slab model. This understanding may be useful as a guide to formulating multi-dimensional, time-dependent numerical simulations to investigate resistive-viscous flows.

ACKNOWLEDGMENTS

We thank Yuhong Fan, Natasha Flyer, Ian Lerche and Gene Parker for comments. One of the authors (A. K. E.) acknowledges a Research Experience for Undergraduate (REU) appointment at the National Center for Atmospheric Research (NCAR) and Colorado University under a National Science Foundation (NSF) REU Grant. NCAR is sponsored by NSF.

Appendix A: The $u \to 0$ singularity

The substitution $\epsilon = h_1 - h > 0$ with $0 < h_1 \leq 1$ transforms ODE (29) into the form

$$\mu_1 u \frac{d^2 u^2}{d\epsilon^2} - 2u + \gamma_1 + 2h_1\epsilon - \epsilon^2 = 0, \tag{A1}$$

with $\gamma_1 = 1 - h_1^2$. Subject to $u = 0$ at $\epsilon = 0$, this ODE admits the solution of the form

$$u = \epsilon f(\epsilon) + \epsilon^{1/2} g(\epsilon), \tag{A2}$$

where $f(\epsilon)$ and $g(\epsilon)$ are assumed to be analytic. Direct evaluation shows that $u\frac{d^2u^2}{d\epsilon^2}$ has the same mathematical form as u, namely, the sum of an analytic function and a product of $\epsilon^{1/2}$ with another analytic function. Therefore, ODE (A1) decomposes into

$$\epsilon f \frac{d^2}{d\epsilon^2}\left(\epsilon^2 f^2 + \epsilon g^2\right) + \frac{1}{2} g \left(4\frac{d^2}{d\epsilon^2}\left(\epsilon^2 fg\right) - fg\right) + \gamma_1 + 2h_1\epsilon - \epsilon^2 - 2\epsilon f = 0, \tag{A3}$$

$$g \frac{d^2}{d\epsilon^2}\left(\epsilon^2 f^2 + \epsilon g^2\right) + \frac{1}{2} f \left(4\frac{d^2}{d\epsilon^2}\left(\epsilon^2 fg\right) - fg\right) - 2g = 0, \tag{A4}$$

to determine $f(\epsilon)$ and $g(\epsilon)$. In the small neighborhood $\epsilon << 1$, solution $u(\epsilon)$ may have the expansions

$$\epsilon f(\epsilon) = \sum_{n=1}^{\infty} a_n \epsilon^n, \tag{A5}$$

$$g(\epsilon) = \sum_{n=0}^{\infty} b_n \epsilon^n, \tag{A6}$$

where a_n and b_n are constant coefficients, noting that the lead term of the series for $\epsilon f(\epsilon)$ is not a constant because $u = 0$ at $\epsilon = 0$. Then, ODEs (A3) and (A4) give two coupled sets of recursive, nonlinear algebraic equations for the coefficients a_n and b_n. The second-order ODE (A1) has two integration constants, one of which has been used to set $u = 0$ at $\epsilon = 0$, so either a_1 or b_0, but not both, may be arbitrarily prescribed to generated all the other expansion coefficients recursively. In ascending powers, $u \approx b_0\epsilon^{1/2} + a_1\epsilon + b_1\epsilon^{3/2} + a_2\epsilon^2 + ...$ showing that u goes to zero at worst as $\epsilon^{1/2}$ with an unbounded gradient, provided $b_0 \neq 0$. Let us assume that the expansions of $\epsilon f(\epsilon)$ and $g(\epsilon)$ have nonzero radii of convergence, a nonlinear property too formidable to attempt a proof here. This assumption seems reasonable based upon the physically sensible numerical solutions obtained.

To second order in ϵ, the decomposition equation (A3) gives

$$a_1 b_0^2 + \gamma_1 = 0, \tag{A7}$$

$$\mu_1\left(23a_2b_0^2+4a_1^3+38a_1b_0b_1\right)+4h_1-4a_1=0, \tag{A8}$$

$$\mu_1\left(47a_3b_0^2+28a_1^2a_2+78a_2b_0b_1+78a_1b_0b_2+35a_1b_1^2\right)-2-4a_2=0, \tag{A9}$$

whereas the decomposition equation (A4) gives

$$b_0\left[\mu_1\left(8b_0b_1+11a_1^2\right)-4\right]=0, \tag{A10}$$

$$\mu_1\left(24b_0^2b_2+20b_0b_1^2+54a_1a_2b_0+27a_1^2b_1\right)-4b_1=0, \tag{A11}$$

$$\mu_1\left(48b_0^2b_3+12b_1^3+80b_0b_1b_2+102a_1a_3b_0+47a_2^2b_0+94a_1a_2b_1+512a_1^2b_2\right)-4b_2=0. \tag{A12}$$

If $h_1<1$, then $\gamma_1=1-h_1^2\neq 0$ and a_1 and b_0 are nonzero by Equation (A7). We may take b_0 to be a freely prescribed parameter to initiate the recursive chain of determination of a_n and b_n for $n>1$. For example, Equations (A7), (A10), (A8), (A11), (A9), (A12) in that order determine, respectively, $a_1, b_1, a_2, b_2, a_3, b_3$, and so on, in terms of b_0.

Those numerical solutions in Figures 2 and 3 vanishing at some interior point $h=h_1<1$ have been computed by integrating toward $h=1$ from $h=0$ where an initial value $u_0=u(0)$ and zero gradient are prescribed. Knowing rigorously that $u\to 0$ at $h=h_1$ as $\epsilon^{1/2}$ is an invaluable guide in our Runge-Kutta numerical computation. This simple singularity permits the numerical integration of $u(h)$ to proceed close to the zero point $h=h_1$ where $u=0$ before the numerical difference-equations representing ODE (A1) break down, with some undetermined inaccuracy in the location of $h=h_1$, as we have pointed out. This inaccuracy in determining h_1 for a given u_0 is tolerable in our purpose of determining the BVP solutions labeled (v) in these Figures that do not vanish in the entire half-domain $0<h<1$. The expansion given by Equations (A7)-(A12) is useful for computing with a higher numerical precision a solution $u(h)$ that does vanish at an interior point. Although such solutions lie outside the scope of our paper, understanding their properties is important in our numerical work.

In any numerical computation, it is helpful to solve a problem in a formulation that avoids extreme numerical values as much as it is possible. For our Runge-Kutta computations of the solution curves displayed in Figures 2 and 3, we avoid the numerical hazards of $u(h)$ having an unbounded gradient at $h=h_1$ by solving ODE (32) for $q=u^2$ that takes the form

$$\mu_1 q^{1/2}\frac{d^2q}{d\epsilon^2}-2q^{1/2}+\gamma_1+2h_1\epsilon-\epsilon^2=0, \tag{A13}$$

on ϵ-space, subject to boundary conditions (33) similarly transformed. We have then the modest advantage that q has a bounded gradient everywhere, including the end point $h = h_1$.

If $h_1 = 1$, then $\gamma_1 = 0$ and recursive equation (A7) requires either $a_1 = 0$ or $b_0 = 0$, defining two independent solutions in the neighborhood of $\epsilon = 0$. Multiple solutions are not a surprise because the governing ODE is nonlinear. The $a_1 = 0, b_0 \neq 0$ solution is the parametric limit of an interior solution vanishing at $h = h_1 < 1$ as $h_1 \to 1$. All such solutions carry the lead term $u \approx b_0\epsilon^{1/2} \equiv b_0(h_1 - h)^{1/2}$ in the neighborhood $\epsilon << 1$. For the BVP in h-space, boundary conditions (31) require $\frac{du^2}{dh} = 0$ for the fluid to be stress-free at $h = 1$, corresponding to $\frac{du^2}{d\epsilon} = 0$ at $\epsilon = 0$ in ϵ-space. The $a_1 = 0, b_0 \neq 0$ solution has no interest for our FBP because $u^2 \approx b_0^2\epsilon$ violates this boundary condition at $\epsilon = 0$.

If $a_1 \neq 0$, then $b_0 = 0$ by recursive equation (A7), from which $b_n = 0$ for all n by other recursive equations. This follows more directly by observing that Equations (A2), (A3), and (A3) admit the possibility of a solution $u(h)$ with $f \neq 0$ but $g \equiv 0$ with $b_n = 0$ for all n. The recursive equations then give a_n with $n > 1$ in terms of a_1 to define f as an infinite series. The derivation shows that a_1 is not a free parameter. With $b_0 = 0$, recursive equation (A10) is satisfied trivially whereas recursive equation (A8) requires a_1 to be a root of the cubic equation

$$\mu_1 a_1^3 - a_1 + 1 = 0. \tag{A14}$$

Therefore, all the coefficients a_n are fixed by the given constant μ_1 that defines the ODE (29) for u. In other words, the local solution defined by a_n as a series in ϵ is a particular solution of ODE (29) uniquely defined by μ_1.

Appendix B: Two-dimensional steady resistive-viscous flows

The 1D steady states of the infinite slab studied in this paper provide a physical motivation to investigate the formidable BVP posed by similar 2D states in the $y - z$ plane. Fig. 10 is a recent 2D generalization of the static KS slab. Let us break the 1D symmetry of the KS slab in Fig. 4 by introducing a periodic variation in the z direction with period L. In each periodic cell of vertical height L and unbounded extension in the two opposite directions in y, we have a total mass of $M_T L$. By redistributing this total mass in a suitable identical manner over each cell and retaining the dipped topology of the field, we obtain the configuration in Fig. 10, which is an exact solution[26] describing a 2D slab in static

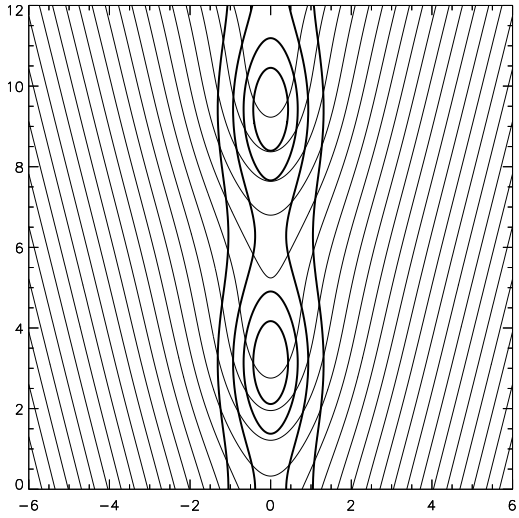

FIG. 10. Two-dimensional generalization[26] of the static KS slab, displaying the dipped (thin) field lines and (thick)contours of constant isothermal density on the $y-z$ plane. The field and density distributions are periodic in the vertical z-direction, two periodic cells shown here. This 2D static equilibrium is created by a suitable identical redistribution of the total mass of the KS slab in Fig. 4 over each of such periodic cells.

equilibrium satisfying

$$\frac{1}{4\pi}(\nabla \times \mathbf{B}) \times \mathbf{B} - \nabla p - \rho g \hat{z} = 0, \tag{B1}$$

$$\nabla \cdot \mathbf{B} = 0, \tag{B2}$$

where p and ρ are related by the isothermal condition (4). The details are not essential in this short Appendix, for Fig. 10 suffices to make two points. The KS slab as a $\mu_1 = 0$ is embedded in a manifold of 2D static slabs of which Fig. 10 shows an example. What are the generalizations of this static 2D example to allow for a $\mu_1 \neq 0$ resistive-viscous flow in the steady state? This generalization is formidable, requiring two steps, going from static equilibrium to steady ideal MHD flows[47,48] and then to allow for resistivity and viscosity. The problem becomes even more interesting if we give up the simplifying isothermal assumption. In this case, the balance of viscous, Lorentz, pressure and gravitational forces is coupled nonlinearly with thermal balance in a 2D steady state in the magnetic geometry in Fig. 10. For the quiescent prominences, thermal balance is dominated by an anisotropic

thermal conduction[2,26] that is efficient along the field but significantly suppressed across the field. This anisotropy results a ready tendency for adjacent magnetic flux tubes of fluid to develop uncorrelated temperature-profiles along their lengths, leading to a discrete pressure jump between the tubes and a compensating magnetic-pressure jump for force balance between the tubes. The latter jump gives rise to such thin current-sheets that must dissipate, producing a viscous-resistive flow of fluid between the flux tubes. This brief analysis points to a rich wealth of nonlinear plasma processes directly relevant to prominence physics[2,10,11,17,18,22,23,25,26].

REFERENCES

[1]Kippenhahn, R., & A. Schlüter 1957, Z. Astrophys. 43, 36

[2]Low, B. C., T. Berger, R. Casini, & W. Liu 2012a, ApJ 755, 34

[3]Landau, L. D., & E. M. Lifshitz 1959. *Fluid Mechanics* (Reading, MA: Addison-Wesley)

[4]Shercliff, J. A. 1953, Math. Proc. Camb. Phil. Soc. 49, 136

[5]Harris, E. G., 1962, Nuovo Cim. 23, 115-121

[6]Low, B. C., & Y. Q. Lou 1990, ApJ 352, 343

[7]Tsinganos, K., & G. Surlantzis 1992, A&A 259, 585

[8]Tandberg-Hanssen, E. 1995, The nature of solar prominences (Dordrecht: Kluwer)

[9]Low, B. C., 2001, JGR 106, 25141

[10]Labrosse, N., P. Heinzel, J.-C. Vial, T. Kucera, S. Parenti, S. Gunar, B. Schmieder, G. Kilper 2010, Space Sci Rev 151, 243.

[11]Mackay, D. H., J. T. Karpen, J.L. Ballester, B. Schmieder, & G. Aulanier 2010, Space Sci Rev 151, 333

[12]Berger, T. E., et al. 2008, ApJ Lett., 676, L89

[13]Berger, T. E., et al. 2010, ApJ 716, 1288

[14]Okamoto, J. T., et al. 2007, Science 318, 1577

[15]Okamoto, J. T., et al. 2008, ApJ 673, L215

[16]Okamoto, T. J., S. Tsuneta & T. E. Berger 2010, ApJ 719, 583

[17]Berger, T. E., et al. 2011, Nature 472, 197

[18]Hillier, A., H. Isobe, K. Shibata & T. Berger 2011, ApJ 736, L1

[19]Leroy, J.-L.1989, in Dynamics and structures of quiescent prominences, ed. E. R. Priest

(Dordrecht: Kluwer)

[20]Casini, R., A. L. Lopez Ariste, S. Tomczyk & B. W. Lites ,2003, ApJ 598, L67

[21]Lopez Ariste, A. L., & R. Casini 2003, ApJ 582, L51

[22]Gilbert, H. R., V. H. Hansteen, & T. E. Holzer 2002, ApJ 677, 464

[23]Gilbert, H. R., G. Kilper, & D. Alexander 2007, ApJ 671, 978

[24]Berger, T. E., Liu, W., & Low, B. C. 2012, ApJ 758, L37

[25]Liu, W., T. E. Berger, & B. C. Low 2012, ApJ 745, L21

[26]Low, B. C., W. Liu, T. Berger & R. Casini 2012b, ApJ 757, 21

[27]Parker, E. N. 1972, ApJ 174, 499

[28]Parker, E. N. 1994, *Spontaneous Current Sheets in Magnetic Fields* (New York: Oxford U Press)

[29]Janse, Å. M., Low, B. C. & Parker, E. N. 2010, Phys. Plasmas 17, 092901

[30]Low, B. C., 2010, ApJ 718, 717

[31]Low, B. C., 2013, ApJ 768, 7

[32]Parker, E. N. 1966, ApJ 145, 811

[33]Parker, E. N. 1967, ApJ 149, 517

[34]Lerche, I. 1967, ApJ 149, 553

[35]Mouschovias, T. C. 1976, APJ 206, 753

[36]Shibata, K., Tajima, T., Matsumoto, R., Horiuchi, T., Hanawa, T., Rosner, R., Uchida, Y. 1989, ApJ 338, 471

[37]Lerche, I., & B. C. Low 1980, ApJ 242, 1144

[38]Low, B. C., & W. Manchester, III 2000, ApJ 528, 1026

[39]Hall, G. 1981, in The numerical solutions of nonlinear prolblems, C. T. H. Haker & C. Phillips (eds.) (Oxford: Clarendon Press)

[40]Press, W. H., S. A. Teukolsky, W. T. Vetterling & B. P. Flannery 2007, *Numerical Recipes* (Cambridge: Cambridge U. Press)

[41]Zweibel, E. G., 1982, ApJ 258, L53

[42]Low, B. C., & S. T. Wu 1981, ApJ 248, 335

[43]Low, B. C., & G. J. D. Petrie 2005, ApJ 626, 551

[44]Haerendel, G. & T. Berger 2011, ApJ 731, 82

[45]Petrie, G. J. D., & B. C. Low 2005, ApJS 159, 288

[46]Zweibel, E. G., & Yamada, M. 2009, ARA&A, 47, 291

[47]Tsinganos, K. 1981, ApJ 245, 761

[48]Tsinganos, K. 1982, ApJ 252, 775